Proceedings of the 2006 IEEE International Conference on Robotics and Automation
Orlando, Florida - May 2006

Cutting, 'by Pressing and Slicing', Applied to the Robotic Cut of Bio-materials, Part II: Force during Slicing and Pressing Cuts

Debao Zhou[*], Mark R. Claffee[+], Kok-Meng Lee[+] and Gary V. McMurray[*]
[*]Food Processing Technology Division, HES Laboratory, Georgia Tech Research Institute, Atlanta, GA 30332
[+]George W. Woodruff School of Mechanical Engineering, Georgia Institute of Technology, Atlanta, GA 30332
Email: {debao.zhou, gary.mcmurray}@gtri.gatech.edu, m.claffee@gatech.edu, kokmeng.lee@me.gatech.edu

Abstract

The applications of robotics are becoming more and more common in non-traditional industries such as the medical industry including robotic surgery and sample microtoming as well as food industry that include the processing of meats, fruits and vegetables. In this paper, the influence of the blade edge-shape and its slicing angle on the cutting of biomaterials are formulated and discussed based on the stress analysis that has been presented in Part I. Through modeling the cutting force, an optimal slicing angle can be formulated to maximize the feed rate while minimizing the cutting forces. Moreover, the method offers a means to predict cutting forces between the blade and the biomaterials, and a basis for design of robust force control algorithms for automating the cutting of biomaterials.

Key words: *robotics, blade cutting, slicing angle, sharpness*.

1. Introduction

Cutting is normally an onerous operation in the food industry, which is required in the processing of meats, fruits, and vegetables. In order to develop automated machines to perform these cutting operations on non-engineering materials, this study attempts to establish a thorough understanding of the science behind cutting of biomaterials. The initial test bed for our development is the wing-shoulder cutting operation in a typical poultry processing plant. This cut is not only difficult for the human operator and very labor intensive, but it is also one that directly affects the yield of the breast meat; the most profitable margin item on a bird. Cutting line workers are at high risk of developing musculoskeletal disorders (MSDs) which are often attributed to the forces, postures and repetition of the processing tasks [1].

During cutting, the formation of the chips (or offcuts) plays a major role in the amount of energy required to result in cutting. Metal cutting creates plastically deformed offcuts which permanently store energy while the elastically deformed food offcuts (in materials such as cheese, fruit, etc) permanently store almost no energy. Thus many researchers have formulated the food cutting problems using the energy method through the application of the fracture toughness concept [2]; among them, Mahvash and Hayward [3] formulated the relationship between the cutting force and cut depth during deformation, cutting, and rupture and Atkins *et al*. [4] explained why there is smaller cutting force requirement when pressing and slicing compared to pressing only. Atkins and Mai provided experimentally determined values for fracture toughness of several bio-materials [5]. Starting from the energy perspective, Kamyab *et al*. [6] formulated the stress and force distribution in cheese cutting. An alternative method based on internal stress has also been used to explain the cutting process. For example, Yoshihara and Matsumoto [7] studied the shearing properties of wood using the stress analysis method, where mainly average shear stress was considered. Through an in-plane shear test of a thin specimen, some of the material properties (such as shear modulus and shear strength) were obtained in [7].

Blade sharpness is also one of the important factors, which affects the required cutting forces. Contact between the cutting object and the blade is an area, which can be shown from the microstructure of a knife. Tech Edge [8] has documented the microstructure of their knife products. Kamyab *et al*. [6] studied the force per unit length of a wire cheese-cutter with various wire diameters and cutting speeds. Blade sharpness also directly influences the cutting moments and the grip forces applied by an operator. McGorry *et al*. [9] studied the magnitude of the grip force and moment using three kinds of blades with different sharpness; namely polished, smooth and coarse knife. They found that a finely polished knife significantly reduced mean grip force and cutting moment during the cutting operation. Szabo *et al*. [10] developed a procedure to establish knife steeling schedules based on increased force due to knife dullness from repetitive use to minimize operator exertions and physical stress associated with work-related musculoskeletal disorders. The cutting area when the blade cut to a carrageenan target is used to quantify the absolute sharpness.

Unlike the above methods that studied the blade sharpness in terms of gripping force, this research uses internal stress to describe the cutting mechanics and the sharpness of a set of blades. Part I of this paper [11] has explicitly developed a stress distribution model, which serves as a basis to explain the cutting principles in this paper. Reference [12] has defined a relative sharpness factor to describe the relationship between the applied force and the knife dullness. This paper provides the analytical expression for the relative sharpness factor. Additionally, other influencing factors (such as edge width and shape) are systematically analyzed. Numerical, simulation and experimental results are used to verify the formulation.

2. Cutting Parameter Analysis

Fig. 1 shows a simplified cutting model and the parameter notations used in this paper. As shown in Fig. 1(a), the cutting force P acts on the surface of a semi-infinite body, where the xy plane is on the boundary of the semi-infinite body; and P_v and P_h are the force components along the z and x directions respectively. The slicing angle α is defined as the angle of P from the positive z direction.

Figure 1(b) illustrates the parameters that characterizes the knife. It is assumed that the knife exerts a constant cutting force along the direction parallel to the *x*-axis and has a cutting force distribution in the *yz* plane shown in Fig. 1(b). The force of the knife has a maximum intensity q at y ∈ [-*s*, *s*] and is linearly reduced to zero at -*a*,and *a*. In the following discussion, the parameters *a* and *s* are referred to as the blade edge-width and blade shape respectively, and the position coordinates (*x,y,z*) are normalized with respect to *a* .

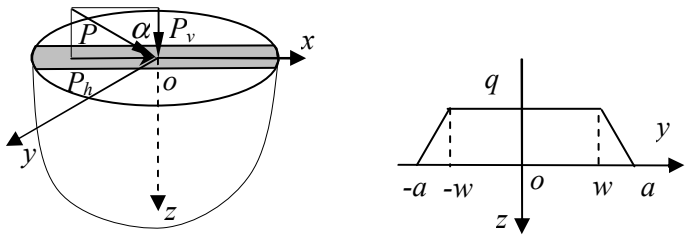

(a) Cutting model, (b) Force distribution in *oyz* plane,
Fig. 1 Cutting force acting on a semi-infinite body.

The assumptions in this part are the same as those in Part I [11] where the cutting stresses are obtained by superimposing the various combinations of the stresses. The cutting stresses are a function of the total force *P*, the contact length *l*, and the knife parameters (*a, s*) as

$$[\sigma]=\begin{bmatrix}\sigma_x & \tau_{xy} & \tau_{xz}\\ \tau_{xy} & \sigma_y & \tau_{yz}\\ \tau_{xz} & \tau_{yz} & \sigma_z\end{bmatrix}=\frac{P}{l(a+w)}\begin{bmatrix}f_1\cos\alpha & f_5\sin\alpha & f_6\sin\alpha\\ f_5\sin\alpha & f_2\cos\alpha & f_4\cos\alpha\\ f_6\sin\alpha & f_4\cos\alpha & f_3\cos\alpha\end{bmatrix} \quad (1)$$

where f_i (i = 1, …, 6) are functions of the ultimate stress τ_u of the material being cut and the knife parameters (*a*, *l*, *w*). When α = 90° (only tangential force acts on the boundary of the semi-infinite body), only τ_{xy} and τ_{xz} are involved. On the other hand, when α = 0° (i.e. only normal force), τ_{xy} and τ_{xz} are zero.

The principle stresses (σ_1, σ_2, σ_3) can be obtained by solving the following eigen-value problem:

$$\boldsymbol{\sigma}\,\mathbf{x} = \lambda\mathbf{x} \quad (2)$$

The principle stresses σ_1, σ_2 and σ_3 and their directions **x** correspond to the eigen-values and eigenvectors respectively. The maximum shear stress can then be obtained as

$$\tau_{mn} = \tfrac{1}{2}(\sigma_m - \sigma_n) \quad (3)$$

where *m* and *n* are 1, 2 or 3.

2.1 Fracture Initialization

Tresca's fracture criterion [14] is used to identify the fracture initialization, which can be expressed as

$$\tau_{\max} = Max[abs(\tau_{12}),\ abs(\tau_{23}),\ abs(\tau_{13})] \ge \tau_u / K_s \quad (4)$$

where τ_u and K_s are the ultimate shear strength, and the notch stress concentration factor respectively. For a given material, τ_u, is assumed to be constant. Two cutting states, pre- and post-fractures, are of interest, during the cutting of the material:

Pre-fracture: As all of the stresses in the material are due to deformation, the notch stress concentration factor, K_s = 1.

Post-fracture: Once the stress reaches the failure criterion given in (4). the criterion K_s = 1 is no longer valid and the stress concentration factor is determined by

$$K_s = \tau_u / \tau_o = F_{Fracture} / F_{Cutting}\ , \quad (5)$$

where τ_u, and τ_o are the ultimate stresses of the pre- and post-fractures respectively.

From (1~3), we have the form:

$$\tau_{mn} = \frac{P}{l(a+s_p)} f_{7mn}(y,z,a,w,\alpha), \quad (6)$$

where the function $f_{7mn}(\ )$ can be explicitly expressed using f_1 to f_6. Consider the fracture that initiates at the location (y_u, z_u), the required force is obtained by substituting (6) into (5),

$$P_u = \frac{\tau_u l(a+w)}{K_s f_8(y_u, z_u, a, w, \alpha)}, \quad (7)$$

where function $f_8(\ )$ can be explicitly expressed using (6). If the relative position between the knife and the material remains unchanged, the position where τ_{max} occurs does not changed. In this case, the relationship between *P* and α can be established. This will be discussed in detail in Section 3.

2.2 Effect of Relative Blade Sharpness Factor

In general, the 'sharpness of a blade' is an approximate measure of the applied force P_u for a given condition (or a specified set of parameters τ_u, *l*, *w*, α). Although it is possible to explicitly express the relationship between these parameters and the external force using (7), it is often impractical to get the exact value of these parameters. A relative sharpness factor η is defined (in the case of the same slicing angle α_c) as

$$\eta = \frac{(a+w)}{K_s f_8(y_u, z_u, a, w, \alpha_c)} \quad (8)$$

Hence, $P_u = l\tau_u\eta = K_u\eta$ (9)

The relative sharpness factor defined in (8) is the extension of the definition that we made earlier in [12], where the sharpness is defined only for "cutting by pressing" or the case α = 0°. Using the concept in [12], the relative sharpness factor can be measured as follows:

First, a nominal blade is selected and its cutting force on a specified material is recorded as P_{u0} .

Next, the corresponding blade sharpness is calculated:

$$\eta_0 = P_{u0} / K_u$$

Then, the relative sharpness of other blades used to cut the same material at a similar condition can be expressed as

$$\eta = \eta_0 P_u / P_{u0}$$

Given the maximum allowable force P_{uf} that can be applied to result in cutting, the dullest sharpness can be defined as

$$\eta_f = \eta_0\, P_{uf} / P_{u0}\ .$$

For convenience, a second parameter, the knife relative sharpness level κ, is defined as

$$\kappa = \text{int}\left(\frac{(n-1)(\eta-\eta_0)}{\eta_f-\eta_0}+1\right),$$

where *n* is a user-defined integer to distinguish the sharpness level of a blade; and int(#) which rounds # to the nearest integer expresses the knife sharpness level. Thus a knife can be categorized into *n*-level of sharpness; level 1 is the relative sharpness level corresponds to η_0 = 1.

3. Simulation Results

The fracture of the material, which is a result of the interaction between the blade edge and the material, depends both on the knife geometry and the material properties. In Section 2, the symbolic expressions of the fracture criteria are given as general rules. The following analysis illustrates the exact mechanism.

3.1 Fracture Force via Slicing Angle

Simulation is performed to examine the effect of the slicing angle. For this simulation, the following parameters are used a = 1, w = 0.85, and P/l = 1. The simulation results for $\alpha = 0°$ and 90° are illustrated in Fig. 2.

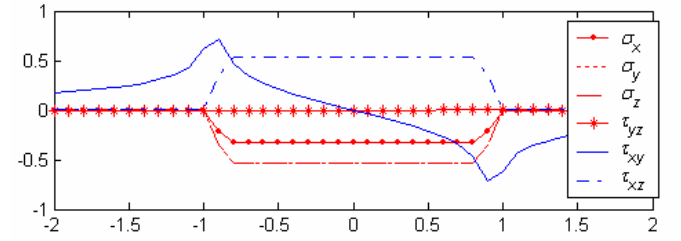

(a) a = 1; w = -w = 0.85a at z = 0;

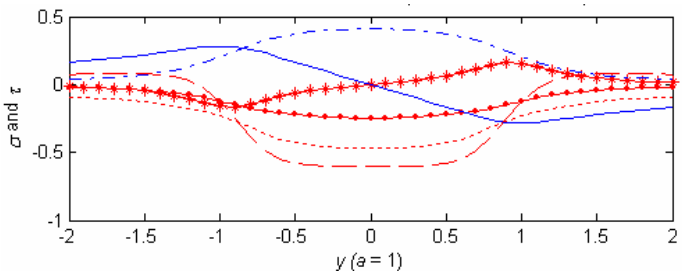

(b) a = 1; w = -w = 0.85a at z = 0.37;

Fig. 2 Stress distribution along y at different z (normalized with P/l).

From Fig. 2, it is found that the maximum stresses occur at four locations which are expressed in (y/a, z/a) and shown in Table 1 as (i) to (iv). Note that the position coordinates (x/a, y/a, z/a) in this paper are normalized to a, half the width of the blade edge (Fig. 1).

Table 1, Locations and values of the possible maximum stresses.

Location	(y/a, z/a)	σ_x	σ_y	σ_z	τ_{xy}	τ_{yz}	τ_{xz}
(i)	(0.00, 0.00)	-0.32	-0.54	-0.54	0	0	0.54
(ii)	(-0.85, 0.00)	-0.32	-0.54	-0.54	0.60	0	0.54
(iii)	(-0.93, 0.00)	-0.15	-0.25	-0.25	0.72	0	0.25
(iv)	(-0.93, 0.37)	-0.14	-0.25	-0.25	0.28	-0.16	0.23

The changes of the maximum stresses, principle stress and maximum shear stress with the slicing angle are shown in Fig. 3(a), (b) and (c), respectively. For clarity, only the stresses at location (ii) are shown in Fig. 3. Other cases have similar trends. As the slicing angle α changes from 0° to 90° at the location (y/a = -0.85, z/a = 0.00), τ_{xy} and τ_{xz} change from 0 to its maximum magnitude, τ_{xy} remains at zero and σ_x, σ_y and σ_z change from their maximum magnitude to 0. The principle stresses change from (-0.32, -0.54, -0.54) to (0.81, 0, -0.81). The maximum shear stresses change from (0.11, 0, 0.11) to (0.81, 0.4, 0.4). Using Tresca's fracture criterion [14] and (9) with K_s = 1, $(\tau_{31})_{max} = \tau_u$ and l =1, the simulated external force P is shown in Fig. 3(d). Similar results for the other three locations are given in Table 1.

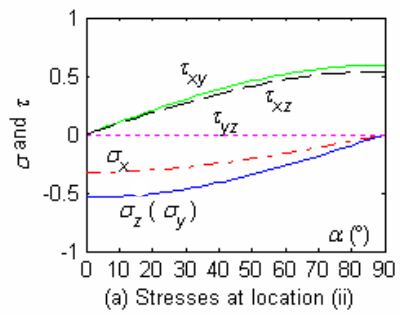

(a) Stresses at location (ii)

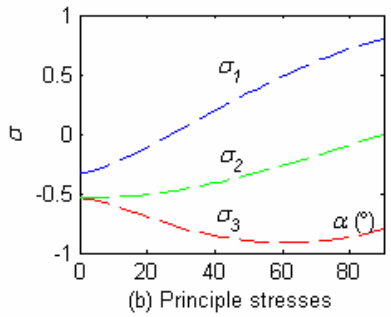

(b) Principle stresses

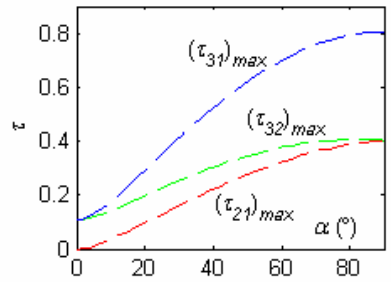

(c) Maximum shear stresses

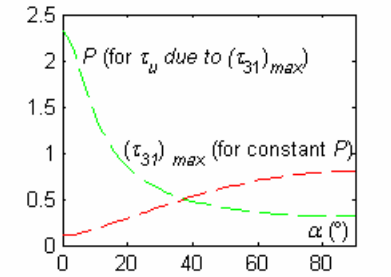

(d) Maximum shear stresses and fracture force

Fig. 3 Stresses and external forces change with slicing angle.

In Fig. 4(a), (i) – (iv) show the location of the maximum shear stress and the corresponding fracture external force, which is the same expression as shown in Fig. 3(d). Note that the maximum shear stresses and the corresponding external force P are shown in the same line style in Fig. 4(a).

Since the external force P is obtained using the same ultimate shear stress τ_u, the smallest one among all the P at the four locations (i) to (iv) will initialize the fracture. It can be observed that when α is from 0° to about 10°, location (iv) will initialize fracture and when α is from about 10° to about 90°, location (ii) will initialize fracture. For clarity, the largest maximum shear stress and its required smallest external force are redrawn in Fig.

4(b). From Fig. 4(b), it can be seen that as the slicing angle changes the required external force will change along the solid black line marked as *P*.

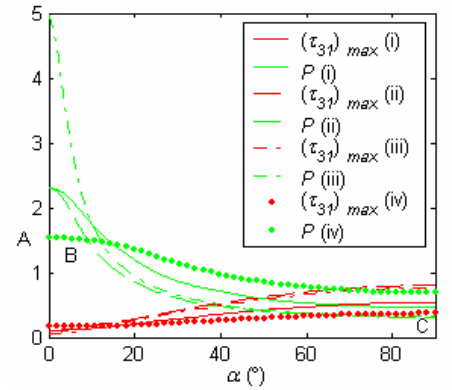

(a)

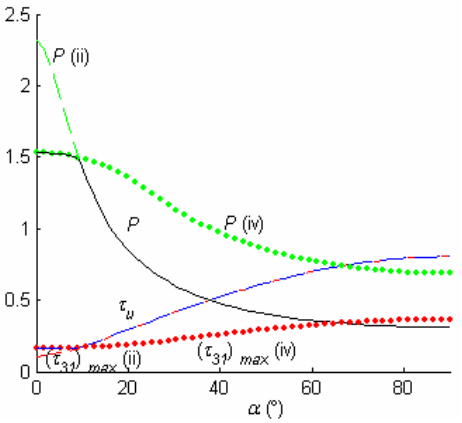

(b)

Fig. 4 Maximum shear stresses and required minimum cutting force.

The total force and its components in the *x* and *z* direction are shown in Fig. 5. It can be seen that the fracture from 0° to about 10° is due to τ_{yz} which is just beneath the surface ($z \neq 0$). It is the mode II fracture, edge-sliding fracture as shown in Fig. 6(a). The fracture from 10° to 90° is due to τ_{xy} and τ_{xz} which is just on the surface ($z = 0$). It is the mode III fracture, out-of-plane tearing, as shown in Fig. 6(b).

From the external force profile shown in Fig. 5, the influence of the slicing angle can be clearly seen. The required force to cut by compression only is far larger than the force required by both compression and slicing. Note also that force P_h does not change greatly in mode III fracture and its value is equal to the total force.

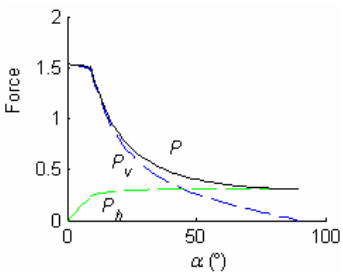

Fig. 5 Total force and the force components in *x* and *z* direction, respectively.

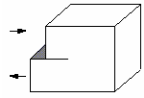

(a) Shearing mode (K_{II}),

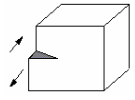

(b) Tearing mode (K_{III}).

Fig. 6 Fracture modes during cutting.

3.2 Fracture Force via Blade Shape

The knife shape can be defined using the parameters *l*, *a*, *w* and *w*. The influence of *l* (contact length) and *a* (edge width) can be directly measured. If *l* and *a* increase, the distributed force intensity will decrease. In order to realize the cut, larger force must be applied as shown in the experimental results in [12]. The influence of the edge shape can be roughly expressed using *w*. Using (2), the stress distribution for the different value of the knife shape parameter *w* on the surface is shown in Fig. 7. From Fig. 7, it is observed that by keeping the external force unchanged, when the force distribution changes from constant intensity to linear intensity, the maximum magnitude of all the induced stresses increases. This leads to an increase in the magnitude of the maximum induced shear stress (by using the same external force). Thus, by assuming τ_u is constant, the external force to realize cutting fracture is reduced, i.e. the knife sharpness is increased.

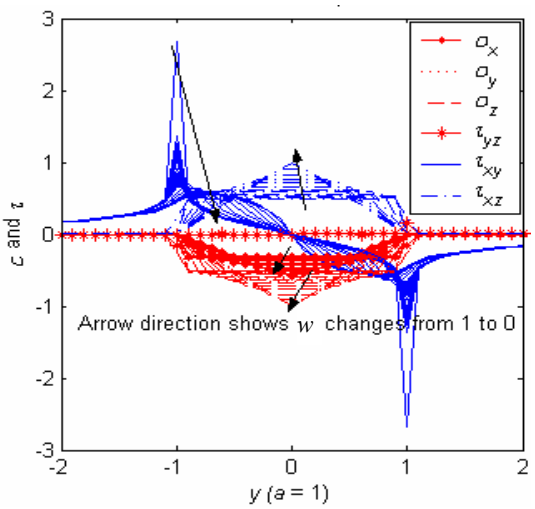

Fig. 7 Stress changes with *w*.

4. Model Validation

In the following, the stress distribution trend is verified using both FEM method and experimental results. Using the results in simulation and the cutting force with slicing angle ($\alpha \approx 90°$), the theoretical cutting force is predicted and compared with the experimental results.

4.1 FEM Verification

ANSYS finite element software was used to provide numerical versification. The properties of the selected material are E = 93259.3 psi and Poisson's ratio ν = 0.25. A large cubic box was used to simulate a half semi-infinite body fixed in the space from its base. A distributed force was added over and area to the middle of the upper surface as shown in Fig. 1.

The stresses for two cases: $\alpha = 0°$ and 90° are shown in Figs. 8 and 9 respectively. Figures 8(a-d) show that when onlyu normal force is applied, τ_{xy} and τ_{xz} are always zero and only σ_x, σ_y, σ_z

and τ_{yz} are non-zero as shown in Fig. 2. The distribution of τ_{yz} in the yz plane is shown in Fig. 8(e). On the other hand, when the force is applied in x direction only Fig. 9 shows that τ_{xy} and τ_{xz} have non-zero values as also shown in Fig. 2.

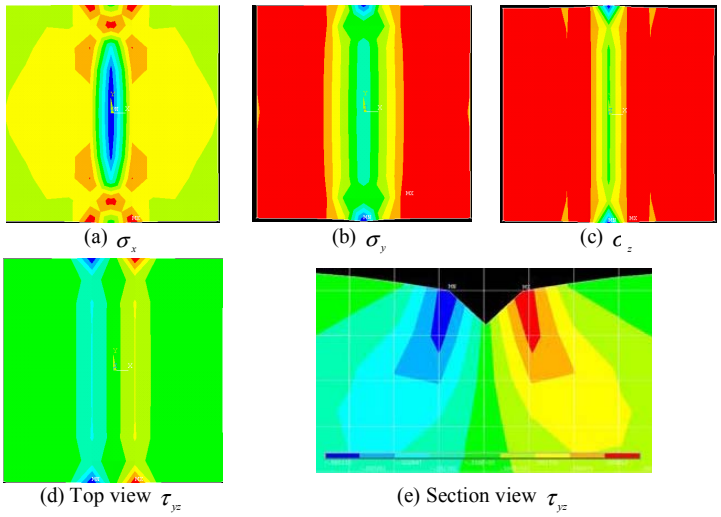

(a) σ_x (b) σ_y (c) σ_z

(d) Top view τ_{yz} (e) Section view τ_{yz}

Fig. 8 Numerical results of the stress distribution with P_v only.

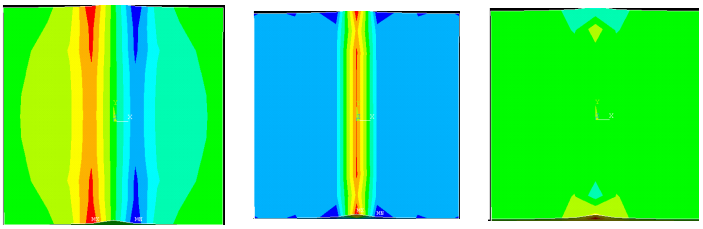

(a) τ_{xy} (b) τ_{xz} (c) σ_z

Fig. 9 Numerical results of the stress distribution with P_h only.

4.2 Experimental Verification

The experimental setup is shown in Fig. 10, which consists of an ABB robot IRB 140 [15] for motion generation, speed control and distance measurement and an ATI Force/Torque sensor [16] for force measurement. The robot is commanded to move at a very low speed (0.5mm/s) for cutting. The force data is saved on a central computer. For the experiments, a baking potato and a chicken breast were selected as test materials. The force trajectory obtained from compression cutting of the potato and chicken breast are shown in Figs. 11 and 12, respectively. The data from different slicing angle cuts on potatoes are summarized in Fig. 13.

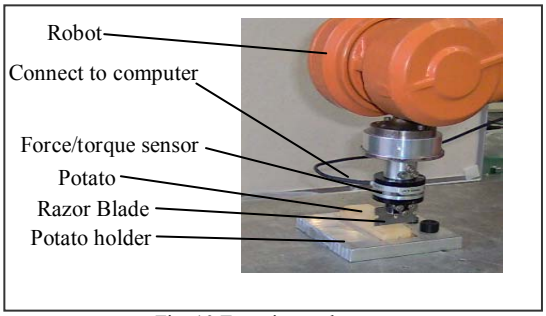

Fig. 10 Experimental setup.

According to the maximum external force when $\alpha \approx 90°$, the ultimate shear stresses at other slicing angle are estimated according to Fig. 5. The experimental data and the theoretical data are shown in Fig. 13. A good match is observed in both force direction. The theoretical forces can then be used as the desired force in the force control loop as shown in Fig. 14 for automating robotic bio-material cutting operations using robotic type devices.

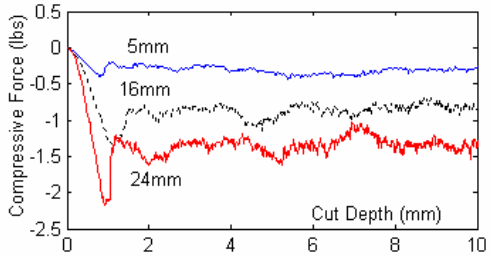

Fig. 11 Force changes with contact length.

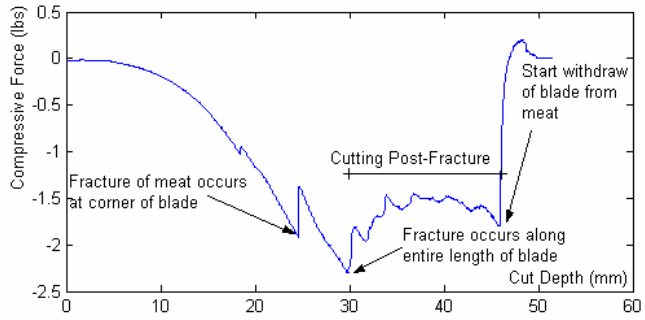

Fig. 12 Force and displacement during chicken meat cutting.

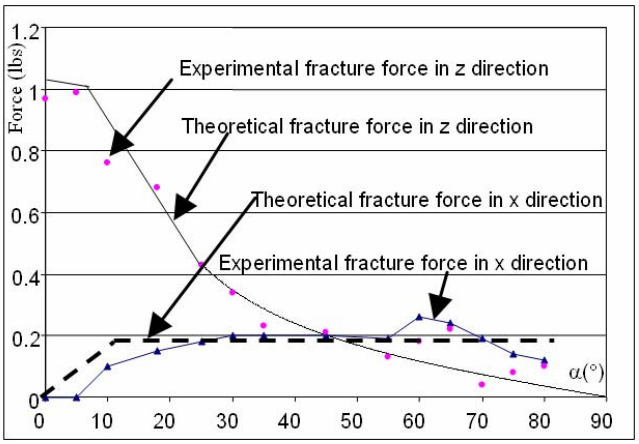

Fig. 13 Experimental data and theoretical estimation of the cutting forces in pressing and slicing cut on potatoes.

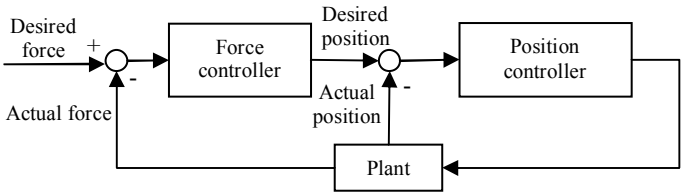

Fig. 14 Illustration of a force control diagram for possible bio-material cutting operation control.

5. Conclusions

Based on the cutting mechanics presented in Part I [11], we investigate the principles of cutting biomaterials. The

relationships between slicing angle, blade edge geometry, contact length, the fracture force, and material properties and the applied force are discussed. Experiments are carried out to validate the formulation.

The following conclusions are drawn: 1) the relationship between the cutting force and internal stress is established. 2) At the initialization of the cutting fracture, the cutting force P is proportional to the contact length l. 3) At the initialization of fracture, the cutting force P is not simply proportional to the width of the blade edge a. Edge shape and edge width have the combined influence on fracture force. For the same edge width, the external force is proportional to the maximum force intensity which the edge shape can generate. 4) For smaller slicing angles, the cutting fracture is due to shear force τ_{yz} (Mode II). For larger slicing angles, the cutting fracture is due to shear force τ_{xy} and τ_{xz} (Mode III). Type III fracture requires considerable less force than Type II fracture. 5) By using the relative sharpness factor concept, blade sharpness can be quantified at certain slicing angles. 6) Based on the material properties, the knife sharpness properties and the interaction between the blade and the material, the required force to realize cutting can be predicted. This observation provides the principle to optimize the cutting mechanism design and the force control algorithm design for the automation of bio-material cutting operations.

In the future, the stress intensity factors K_{II} and K_{III} will be analyzed and quantified. The influence of the knife relative velocity to the material will also be investigated. This work is to provide the foundation for the development of a control system for robotic cutting of natural product.

References

[1] P. G. Dempsey and R. W. McGorry, Investigation of a pork shoulder deboning operation, *Journal of Occupational and Environmental Hygiene*, vol 1, pp. 167-172, 2004.

[2] K. Hellan, *Introduction to Fracture Mechanics*, McGraw-Hill Book Company, New York, 1984.

[3] M. Mahvash and V. Hayward, Haptic Rendering of cutting: A fracture Mechnics Approach, *Haptics-e*, vol. 2, no. 3, pp. 1-12, 2001.

[4] A. G. Atkins, X. Xu and G. Jeronimidis, Cutting, by 'pressing and slicing,' of thin floppy slices of materials illustrated by experiments on cheddar cheese and salami, *Journal of Materials Science*, Springer Science + Business Media B.V., Formerly Kluwer Academic Publishers, vol. 39, pp. 2761– 2766, 2004.

[5] A. G. Atkins and Y. W. Mai, *Elastic and Plastic Fracture: Metals, Polymers, Ceramics, Composites, Biological Materials*, Chichester: Ellis Horwood; New York: Halsted Press, 1985.

[6] I. Kamyab, S. Chalranarti and J.G. Williams, Cutting cheese with wire, *Journal of Materials Science*, vol. 33, pp. 2763-2770, 1998.

[7] H. Yoshihara and A. Matsumoto, Measurement of the shearing properties of wood by in-plane shear test using a thin specimen, *Journal of International Academy of Wood Science*, Springer-Verlag, London, UK, pp. 1-14, 2005.

[8] http://www.furitechnics.com.au/information/Tech%20Edge/Cutting%20edge%20angles.htm, 2005.

[9] R. W. McGorry, P. C. Dowd and P. G. Dempsey, The effect of blade finish and blade edge angle on forces used in meat cutting operations, *Applied Ergonomics,* Elsevier publications, vol. 35, pp. 71-77, 2005.

[10] R. L. Szabo, R. G. Radwin and C. J. Henderson, The influence of knife dullness on poultry processing operator exertions and the effectiveness of periodic knife steeling, *American Industrial Hygiene Association Journal*, Taylor & Francis publications, vol. 62, no. 4, pp. 428-433, 2001.

[11] D. Zhou, M. Claffee, K.-M. Lee and G. McMurray, *Cutting, 'by Pressing and Slicing', Applied to the Robotic Cut of Bio-materials, Part I: Modeling of Stress Distribution*, in the Proceedings of the IEEE International Conference on Robotics and Automation (ICRA06), May 2006.

[12] D. Zhou, M. Claffee, K.-M. Lee and G. McMurray, "*Modeling Compression Cutting of Biomaterial for Robot Control*", in the Proceedings of the 2005 ISTED International Conference on Robotics and Application, paper# 498-064, Hilton Hotel@MIT, Boston MA, Oct, 2005.

[13] M. Sadd, *Elasticity: theory, applications, and numerics,* Elsevier Butterworth-Heinemann, Burlington, MA, 2005.

[14] L. Charlles and J. Robert, *Handbook of stress and strength: Design and material applications*, The Macmillan Company, New York, 1963.

[15] *Product Manual IRB 140*, ABB Robotics Products AB publication, article number: 3HAC 7564-1 issue: M2000, 2000.

[16] *Installation and Operations Manual for ISA F/T-16*, ATI Industry Automation Inc. publication, Manual PN 9610-05-1012-04, 1998.